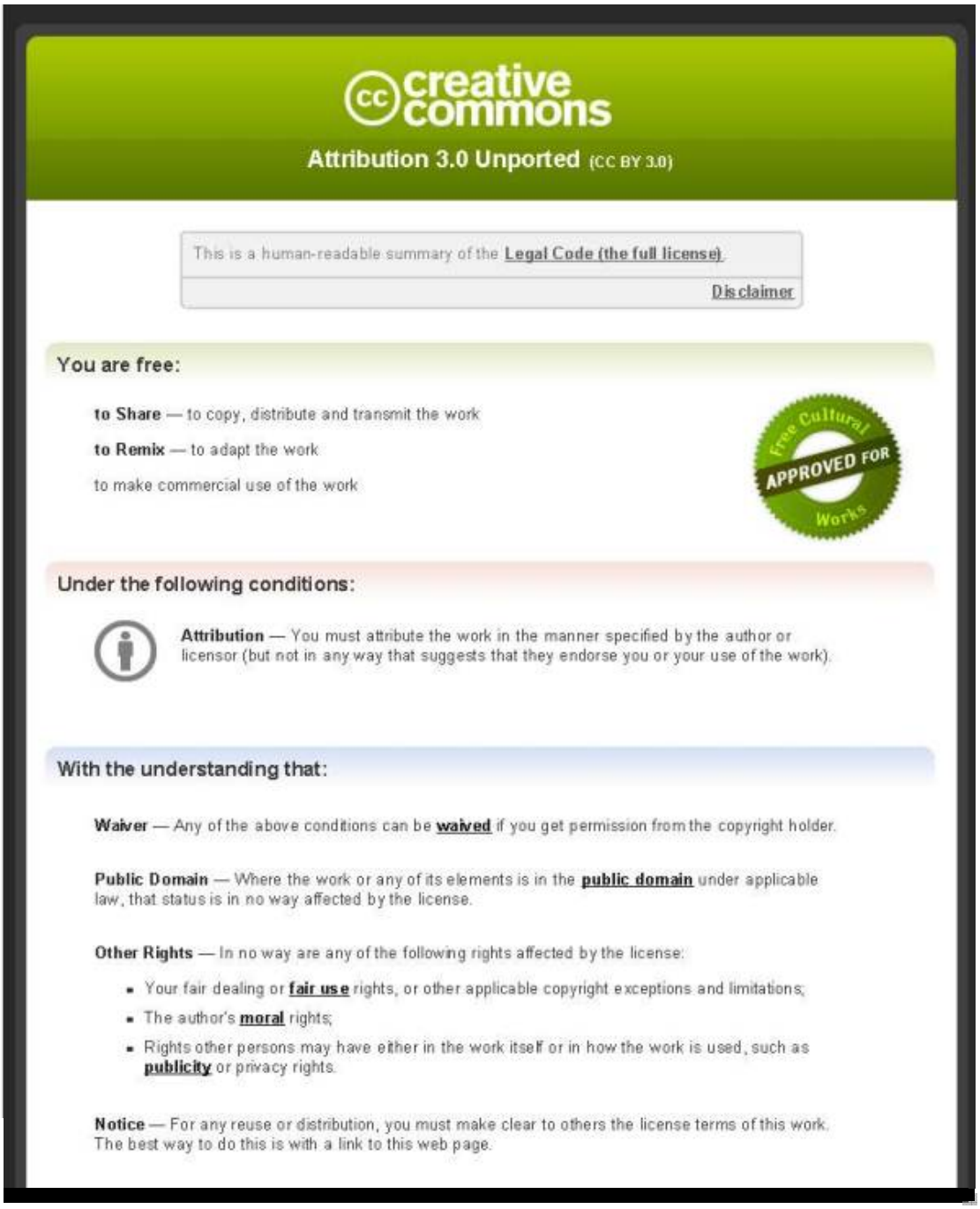

Journal of Biomechanics 47 (2014) 625–630

Contents lists available at ScienceDirect

Journal of Biomechanics

journal homepage: www.elsevier.com/locate/jbiomech
www.JBiomech.com

Changes in the stiffness of human mesenchymal stem cells with the progress of cell death as measured by atomic force microscopy ☆, ☆☆

Nikolay I. Nikolaev [a], Torsten Müller [b], David J. Williams [a], Yang Liu [a,*]

[a] Centre of Biological Engineering, Wolfson School of Mechanical & Manufacturing Engineering, Loughborough University, Loughborough LE11 3TU, UK
[b] JPK Instruments Limited, Unit 7223, Cambridge Research Park, Waterbeach, Cambridge CB25 9TL, UK

ARTICLE INFO

Article history:
Accepted 2 December 2013

Keywords:
Atomic Force Microscopy (AFM)
Stem cells
Elastic modulus
Cell death
Nanoindentation

ABSTRACT

This note reports observations of the change of stiffness of human mesenchymal stem cells (hMSCs) with the progress of cell death as measured by AFM. hMSC with impaired membrane, dead and viable cells were labelled with Annexin V and Propidium Iodide after 24 h cold storage, followed by AFM measurement and Young's modulus of cells was derived. Viable hMSCs have a Young's modulus (E) in the range of 0.81–1.13 kPa and consistent measurement was observed when different measurement locations were chosen. E of cells with partially impaired membrane was 0.69 ± 0.17 kPa or in the range of 2.04–4.74 kPa, depending upon the measurement locations. With the loss of membrane integrity, though there was no variation on measured E between different locations, a mixed picture of cell stiffness was observed as indicated by cells with E as low as 0.09 ± 0.03 kPa, in a mid-range of 4.62 ± 0.67 kPa, and the highest of up to 48.98 ± 19.80 kPa. With the progress of cell death, the highest stiffness was noticed for cells showing a more granular appearance; also the lowest stiffness for cells with vacuole appearance. Findings from this study indicate that cell stiffness is significantly altered with the progress of cell death.

1. Introduction

The influence of aging (Zahn et al., 2011; Lieber et al., 2004; Starodubtseva, 2011), disease pathophysiology (Lee and Lim, 2007) and chemotherapy (Targosz-Korecka et al., 2012) on the mechanical properties of primary and cancer cells (Fuhrmann et al., 2011) have been investigated by micro-rheological measurements using magnetic particles, measurement of elasticity using AFM, micropipette aspiration, and optical stretching (Di Carlo, 2012). Differences in cell mechanical properties of malignant and benign breast tumours have also been observed (Li et al., 2008), and furthermore cancer cells with a highly invasive phenotype (Hur et al., 2011), or immortalised cells (Lulevich et al., 2010), have shown different deformability when compared to primary cells. All these findings have inspired further research in label-free biophysical measurement using lab-on-chip technology to demonstrate the possibility of cell classification based on deformability used as a mechanical biomarker (Hur et al., 2011; Di Carlo, 2012).

With the development of stem cell technology, it has been recognised that cell mechanical properties are correlated with not only aging and pathophysiology of diseases but also the differentiation potential of stem cells (Gonzalez-Cruz et al., 2012). Morphological change of apoptotic cells (Hessler et al., 2005; Wang et al., 2011) and change in the mechanical properties of stem cells after osteogenic (Titushkin and Cho, 2007) and cardiac differentiation (Tan et al., 2012) have been demonstrated by AFM measurement. Our previous work (Nikolaev et al., 2012) has shown the synergistic effect of cold storage duration and vibration-induced mechanical cell damage. It is well known that prolonged cold storage induces apoptotic and necrotic cell death, but it is still not clear whether cell stiffness is also altered with the progress of cell death, hence, leading to susceptibility to mechanical cell damage. To correlate the progress of cell death with mechanical damage, in the current study AFM nano-indentation was applied to identify the stiffness of single suspended viable, dead and membrane-impaired hMSCs after cold storage. Further, all of the reported AFM measurements to date have only been carried out on immobilised cells or cells anchored to substrates. This study is the first time that AFM measurements of single suspended cells have been achieved without using any immobilisation technique to show the stiffness differences consequent on the progress of cell death.

☆☆We are submitting this work as an Original Article. We can confirm that all authors were fully involved in the study and preparation of the manuscript and that the material within has not been and will not be submitted for publication elsewhere.

* Corresponding author. Tel.: +44 1509227602; fax: +44 1509227648.
E-mail address: y.liu3@lboro.ac.uk (Y. Liu).

0021-9290/$ - see front matter © 2013 The Authors. Published by Elsevier Ltd. All rights reserved.
http://dx.doi.org/10.1016/j.jbiomech.2013.12.004

2. Materials and method

2.1. Cell suspension preparation for AFM

hMSC suspensions were prepared following the same procedures as in our previous work (Nikolaev et al., 2012). Bone marrow-derived hMSCs (Lonza) suspensions collected at passage 5 and stored in a fridge overnight were used for AFM (CellHesion® 200, JPK, Germany) measurement of single cell elastic modulus. Annexin V apoptosis analysis (Invitrogen, UK) was applied after the cold storage and before imaging to identify cells with impaired membranes (Annexin V+, Propidium Iodide (PI)−), dead cells (Annexin V+ and PI+), and viable cells (Annexin V−, PI−). Bright field and fluorescence images were taken with an Imaging Source camera under comparable exposure conditions of 67 ms and 550 ms, respectively.

2.2. AFM measurement of single cell mechanical properties

The AFM (CellHesion® 200, JPK, Germany) was combined with an inverted fluorescent microscope (AxioObserver, Zeiss) with Hg-lamp illumination to localise cells at different stages of death as indicated by the fluorescent staining of Annexin V apoptosis analysis and to guide the position of the tip of an AFM cantilever. Cell compression was accomplished at room temperature and in the presence of fluorescent dyes.

An MLCT AUHW cantilever (Bruker Corp.) with a nominal spring constant of $k=0.06$ N/m, and with 35° front and side angle and pyramidal tips of 2.5–3.5 μm was positioned above the selected cell and the tip approached the cell from a height of several microns. Force calibration of the sensitivity of the individual cantilever was achieved by using a thermal noise method within the JPK integrated software. Compression of selected single cells was carried out through the steps of approach, contact and retraction, and force versus distance curves were obtained for the corresponding steps. The CellHesion® 200 is a tip scanner with an extra long z-working range of up to 100 μm. The typical approach/retract settings were identical with a 10 μm extend/retract length, a pixel rate of 2048 Hz and a speed of 2 μm/s. The system was operated under closed loop control. After reaching the contact force selected the cantilever was retracted. In all cases the retraction length of 10 μm was sufficient to overcome any adhesion between tip and sample, and to make sure that the cantilever was completely retracted from the sample surface.

Young's modulus was derived by fitting curves extracted from 10 to 20 measurements on two locations on a single cell with a Hertz model. Typically, a contact force between 1 to 5 nN, and a speed of 2 μm/s was applied. The standard approach was to probe the geometric centre of the cell first. The adjustment of the position of the cantilever above the sample was carried out under the microscope by controlling the position of the AFM-Head via micrometre precision screws. Usually, the second probe location was selected 2–3 μm away from the first position, or one bleb on the cell surface observed was selected as the second position.

2.3. Data analysis

The Hertz model is based on the assumption that samples are isotropic linear elastic solids and that the indentation depth is much smaller than the characteristic radius of the body (Rosenbluth et al., 2006). Such an assumption is usually not adequately met for individual cells due to the presence of structural components and spatial heterogeneity, especially for anchored cells (Jacobs et al., 2013). However, in the current study an individual cell in suspension was used and the spatial variation due to the presence of stress fibres in the cytoskeleton of anchored cells was avoided. Diameters of suspended viable hMSCs were in the range of 10 to 13 μm, consequently the small indentation assumption was valid for the indentation depth of 400 nm, equivalent to less than 4% of the height of the cells, and could be treated as having infinite depth and width. In this study the selection of indentation depth of about 400 nm also ensured clearance between the cantilever and the surface of the cell (Harris and Charras, 2011).

The original Hertz model was an approximation for the elastic contact and small deformations of two spheres in contact. In the AFM literature, however, the term is often used to refer to a family of different models that have been adapted for simple indentation geometries. The key parameter that is usually adapted is the radius of the contact region for a pyramidal indenter, in this case the Bilodeau model was used (BILODEAU, 1992). Since the Hertz models also have circular symmetry, a further approximation was made for an ideal regular four-sided pyramid square-shaped tip through a modification to the cone model with an effective radius of contact $a=0.709\delta \tan\alpha$ (Rico et al., 2005; JPK Instrument AG, 2012) and the following equation used to process the data.

$$F = 0.7453\frac{E}{1-\nu^2}\delta^2 \tan\alpha$$

where F is force, E is Young's modulus, ν is Poisson's ratio, δ is indentation (tip sample separation), and α is face angle of a pyramid.

Usually a Poisson's ratio of 0.3 (soft tissue), 0.4 or 0.5 (an incompressible material) is used and the best-match of experimental and modelling data has been reported when both cytoplasm and nucleus are treated as incompressible (Ofek et al., 2009), thus a Poisson's ratio of 0.5 was applied in the data analysis for the current study. The curve is fitted using a least squares fit with the Levenberg–Marquardt algorithm. The contact point, baseline and Young's modulus values are all fitted simultaneously. Since the contact point is a crucial parameter, the extend curve is generally used. In some cases there is a tilt in the baseline that is corrected by the function of "Offset And Tilt Correction" built into the JPK data processing software usually up to 2 μm away from the contact point.

3. Results and discussion

Whilst most of the research on the mechanical properties of a single cell has measured when cells are attached to surfaces, Hur et al., propose that single cells in suspension behave more like viscous droplets rather than rigid elastic objects (Hur et al., 2011). Also, when compared to cells attached to substrates, suspension cells are much sub-cellular homogenous due to the lack of cytoskeletal tension fibres and there should be little lateral dependence of measured Young's modulus. However, the validity of the assumption that the cell is a homogenous object depends on the indentation depth and with the increase of indentation depth this assumption becomes less valid due to the presence of cellular components and compliance of sub-cellular layers, especially the cortical actin organisation, and this could result in a variation of Young's modulus observed (Kasas et al., 2013). To avoid such situations, spherical indenters were initially used to apply force to a wider sample area to obtain an overall perspective of the behaviour of the whole cell body. To avoid any artificial effect from non-controllable bias, a total of 33 cells were measured 10–20 times at one or two locations on the cell membrane surface. Analysis from 166 data points (see the online supplementary materials Fig. S1) indicated the change of cell stiffness with the progress of cell death and the awareness of variation of stiffness with the location of measurement for early apoptotic and blebbing cells (300–500 Pa and 1100–1500 Pa). In order to capture information at a higher resolution and with more precise control of location on single cells, the pyramidal indenter was applied at different locations (Harris and Charras, 2011). Hence, the pyramidal indenter fitted the Hertz model with a small indentation no larger than 400 nm was used to derive the stiffness of cells rather than those determined from a large indentation.

Typical examples of force distance curves of indentation for viable cells and stiffer, least stiff and stiffest cells within the sub-

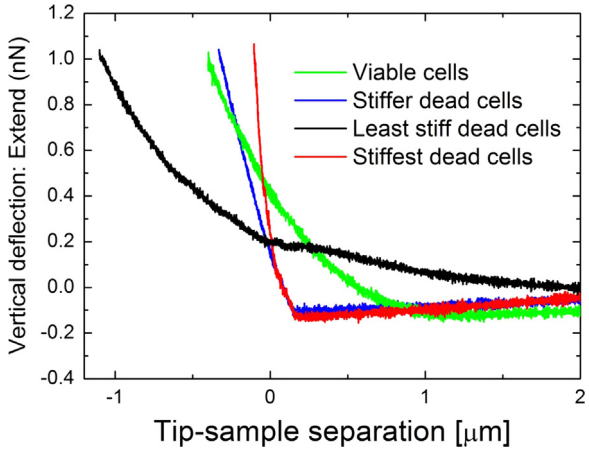

Fig. 1. A typical force distance curve measuring the stiffness of a human mesenchymal stem cell. Working from the right hand edge, the linear portion shows the approach of the cantilever followed by its deflection when in contact with the cell. This shows the stiffness of viable cells, and stiffer, least stiff and stiffest cells within the sub-population of dead cells.

population of dead cells are shown in Fig. 1 with the *Y*-axis labelled as Vertical Deflection Extend. It is clear that different profiles of force versus distance curves are given by different sub-populations of dead cells. To further quantify cell stiffness, all of the analysis of Young's modulus used data from the curve such as those shown in Fig. 1 as these best represent the behaviour of the structure of the parts of the cell membrane and body encountered by the indenter.

Table 1 shows that viable hMSCs have a Young's modulus in the range of 0.81–1.13 kPa, which also falls within the range of 2.5 ± 1.8 kPa reported by Darling et al. (Darling et al., 2008) and consistent measurement was observed even when different measurement locations were chosen. Tables 2 and 3 present the mechanical properties of cells with impaired membrane and dead cells. Among the hMSCs analysed, different intensities of Annexin V and PI staining were observed, showing cells with different extents of membrane damage. The mechanical properties of cells with impaired membranes, as indicated by Annexin+ and PI−, depended on the location of the measurement. Very weak green fluorescence was observed on membrane-impaired cell 1 indicating a small number of phospholipid phosphatidylserines (PS) present on the cell surface and some membrane impairment. The measurement of Young's modulus of membrane-impaired cell 1 was 0.69 ± 0.17 kPa for location A and 4.74 ± 1.06 kPa for location B (see Table 2). Membrane-impaired cell 2 showed slightly stronger green fluorescence, but was still PI impermeable, indicating more cell membrane impairment, but still with membrane integrity. The variation of Young's modulus of membrane-impaired cell 2 with measurement location was also observed, 0.68 ± 0.18 kPa at location A and 2.04 ± 0.19 at location B.

With the loss of membrane integrity as indicated by red fluorescence of PI positive cells, shown in Table 3, though there was no variation on measured Young's modulus between different locations, a mixed picture of cell rigidity was observed. Young's moduli of sub-population of dead cells were measured as 0.09 ± 0.03, 4.62 ± 0.67 and 48.98 ± 19.80 kPa. Young's modulus of dead cell 2 was within the range measured for the stiffer location of cells with impaired membranes. Dead cell 3 was the stiffest cell measured with a very high standard deviation and when correlating with fluorescent and phase contrast images, the strongest Annexin V green fluorescent staining and PI staining were observed and the cytoplasma appeared more granular. In contrast to dead cell 3, dead cell 1, the least stiff among those cells measured, presented a vacuole appearance with also strong Annexin V green fluorescent staining, but very weak PI staining and little granularity.

The schematic diagram shown in Fig. 2 summarises Young's moduli of the cell populations investigated and their corresponding cell membrane status. In general, it is clear that the progress of cells from live (bottom panel of Fig. 2) to membrane impaired (middle panel of Fig. 2) and eventually dead cells (top panel of Fig. 2) was also associated with change of Young's modulus (E) of the cell and a transition from uniform to laterally heterogeneous mechanical compliance across the membrane of single cells and ultimately heterogeneous stiffness for different sub-populations of dead cells. AFM has also been applied to correlate qualitatively the membrane roughness (Wang et al., 2009; Wang et al., 2011) and apoptotic volume decrease (Hessler et al., 2005) with cell apoptosis. The application of AFM to quantify change of total cell volume decrease in the early apoptotic cells has indicated the decrease of total cell volume as early as 16 min after contact with the apoptosis inducer, which proceeds phosphatidylserine translocation from the cytosolic side to the outer surface of the cell membrane (Hessler et al., 2005). In the current study the variation of estimated Young's modulus of Annexin V positive cells with the measurement locations chosen confirmed the heterogeneous lateral distribution of stiffness across the cell surface due to the translocation of membrane phosphatidylserine from the cytosolic side to the cell surface as indicated by the patches of Annexin V positive observed on the cell membrane (see Table 2 column 3). Note that when the whole cell membrane was Annexin V positive, such a variation was not observed and Young's modulus was independent of the location tested. Some influence on cell mechanical properties has been observed when fluorescent dyes are used as cell trackers and it has been suggested that the increase of cell stiffness may be due to the incorporation of the molecules of such dyes into the phospholipid bilayer leading to an increase in the cell Young's moduli (Lulevich et al., 2009). The fluorescent dyes used in the current research were membrane impermeable and the patchy green fluorescence observed is due to the binding of phosphatidylserine on the cell surface with fluorescent labelled Annexin V. Therefore, it is unlikely that such a binding of protein molecules at the cell surface could lead to change of phospholipid bilayers in this experimental arrangement and the variation of cell stiffness with location tested. Yet, such a

Table 1
Mechanical properties of viable cells (both Annexin V− and PI−). For details of axes and labels of Young's modulus distribution see Fig. S2 in online supplementary materials.

Sample ID	Phase contrast	Green (Annexin)/Red (PI) Fluorescence	Young's Modulus ± Standard Deviation (kPa)
Viable cell 1	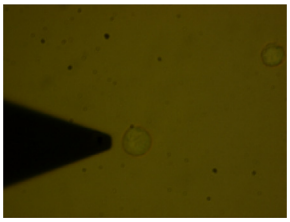	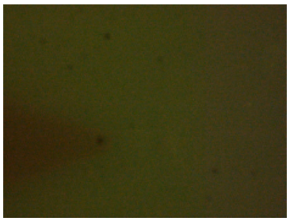	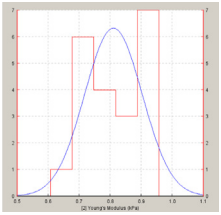 **0.81 ± 0.09**
Viable cell 2	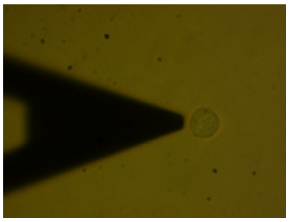	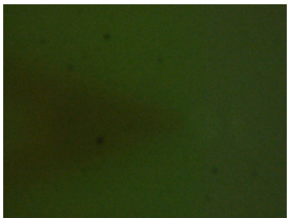	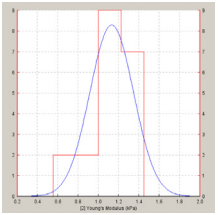 **1.13 ± 0.22**

Table 2
Mechanical properties of cells with impaired membrane (Annexin V+ and PI−). For details of axes and labels of Young's modulus distribution see Fig. S3 in online supplementary materials.

Sample ID	Phase contrast	Green (Annexin) fluorescence	Red (PI) fluorescence	Young's modulus ± standard deviation (kPa)
Membrane-impaired cell 1	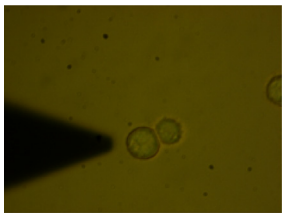	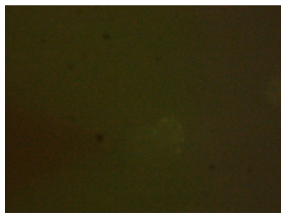	Negative	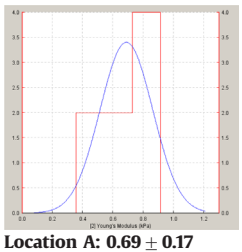 Location A: 0.69 ± 0.17 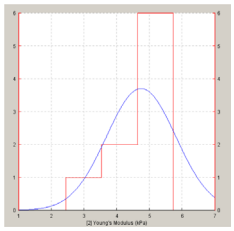 Location B: 4.74 ± 1.06
Membrane-impaired cell 2	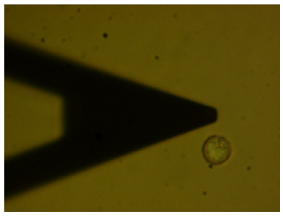	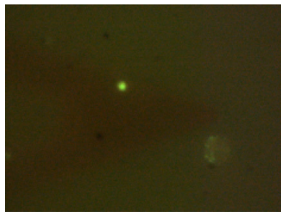	Negative	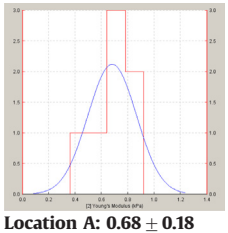 Location A: 0.68 ± 0.18 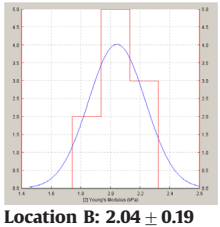 Location B: 2.04 ± 0.19

heterogeneous distribution of the stiffness of the plasma membrane has also been observed for Chinese hamster ovary cells as reported recently by Chopinet et al. (2013). As it has also been reported that cells compressed by the AFM tips can also form mechanically induced blebs (Hemsley et al., 2011), an irregular bulging and protrusion of the plasma membrane, and most recently it was found further that cell stiffness was increased in blebbing vs. non-blebbing cells (Abdelhady et al., 2013), it could also be possible that the lateral variation in cell stiffness observed in the current research was a result of cell blebs.

With the further progress of cell death as indicated by the PI positive staining as a consequence of loss of membrane integrity, the highest stiffness was noticed for cells presenting a more granular appearance; also the lowest stiffness was observed for cells with vacuole appearance (see the top panel of Fig. 2). Cell granularity is a measure of the number of cytoplasmic particles present including mitochondria, ribosomes and other organelles. As the time scale of each indentation was short and hMSCs are anchorage dependent, the investigated cells would not be able to grow at room temperature when kept in suspension state. Thus, it is very unlikely that the change of stiffness was due to reorganisation of the sub-cellular structure in response to the indentation stress. Hence, combining with the low intensity of PI staining of DNA and RNA, the lowest stiffness observed could be a consequence of leaking of cytoplasma and organelles due to membrane rupture.

An increase of nearly two orders of magnitude in cell stiffness has been observed with the progress of chemotherapy-induced cell death of leukaemia cells as reported by Lam et al. (Lam et al., 2007) when measured by AFM, a similar level of increase of cell stiffness was also observed here for the dead hMSCs with the highest stiffness. Nawaz et al. (Nawaz et al., 2012) have stated that the stiffness of attached cells measured by AFM increases with a higher indentation depth due to the presence of the cytoskeleton underlying the cell membrane, but in the current study, the stiffness of suspended cells was measured and stress fibres are absent when cells are in suspension. Hence, the dramatic increase in stiffness was not due to the presence of stress fibres and is most likely due to dynamic changes of cortical actin organisation beneath the cell membrane (Lam et al., 2007; MacQueen et al., 2012). Since the process of cell body disintegration also depends on the mode of cell death, the two extreme moduli of cells measured within the sub-population of dead cells could also be the consequence of different modes of death, i.e. apoptosis via necrosis, as indicated by the decrease in stiffness of chemical-induced apoptotic lymphocytes reported by Hu et al. (2009). In

Table 3
Mechanical properties of dead cells (Annexin V+ and PI+). For details of axes and labels of Young's modulus distribution see Fig. S2 in online supplementary materials.

Sample ID	Phase contrast	Green (Annexin) fluorescence	Red (PI) fluorescence	Young's modulus ± standard deviation (kPa)
Dead cell 1	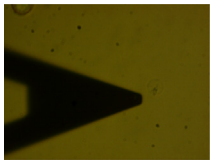	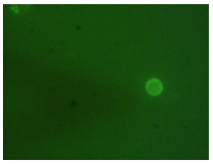		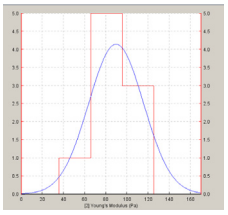 **0.09 ± 0.03**
Dead cell 2	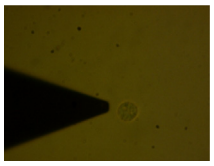	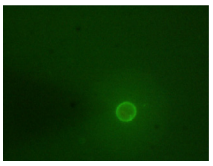		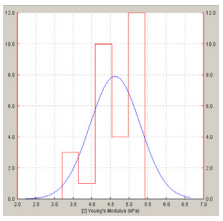 **4.62 ± 0.67**
Dead cell 3	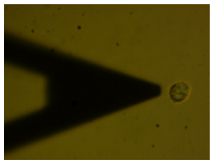	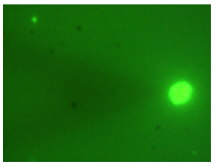	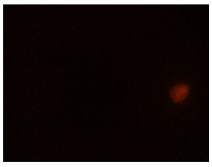	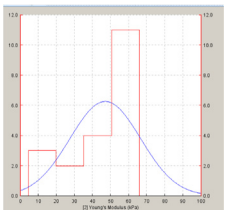 **48.98 ± 19.80**

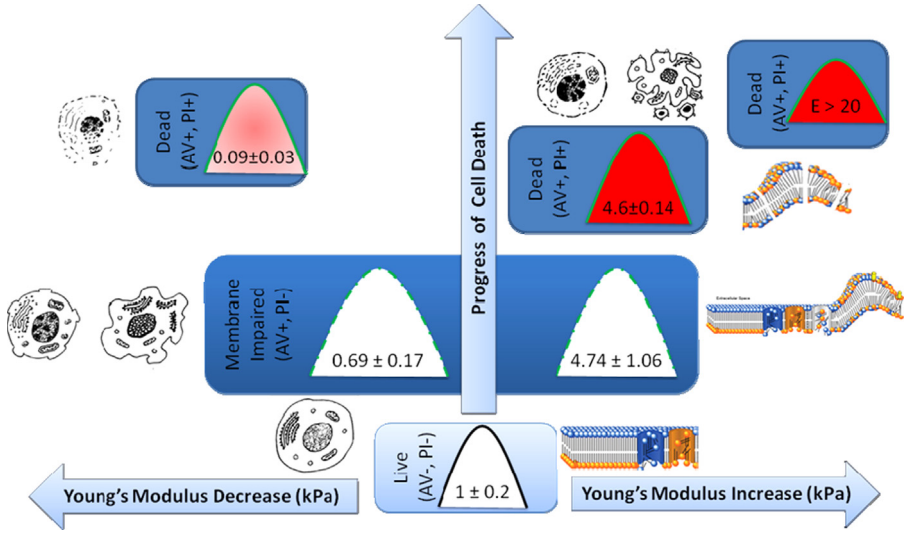

Fig. 2. Schematic diagram shows Young's modulus and corresponding cell membrane status of live, membrane-impaired and dead cells. The image of cell membrane structure and cell body is courtesy of Blankenberg http://www.landesbioscience.com/journals/cbt/04BlankenbergCBT7-10.pdf and Meer et al. http://www.springerimages.com/Images/RSS/1-10.1007_s10103-009-0723-y-0.

addition, as cell volume can decrease dramatically with the progress of cell death (Bortner and Cidlowski, 2002) (the diameter of dead cells measured by Countess Operation Software in the current study was 5–6 μm), the possibility that 400 nm indention depth could violate the Hertz model cannot be excluded for the dead cells as indicated by the higher standard deviation obtained with the stiffest cells. Hence, further modelling work should focus on understanding the relationship of the growth of the size of the indented area with load in order to validate whether the Hertz model holds for dead cells (Johnson, 1985).

Other workers have quantified the change of mesenchymal stem cell stiffness with increased population doubling in order to identify mechanical markers for sub-populations (Maloney et al., 2010). Recently, surface anchoring techniques have also been applied to quantify rigidity difference between single suspended cells and round mitotic cells (Shimizu et al., 2012). This paper presents for the first time AFM measurement of mesenchymal stem cell mechanics without involving any cell immobilisation techniques using cell probes or microfluidic devices. Combining the response of cells to different vibration-induced mechanical

stress during cold transportation observed in our previous work (Nikolaev et al., 2012), recent findings on the impact of temperature on cell mechanics (Kiessling et al., 2013), and the outcomes from the study reported here confirming that cell stiffness is also altered with the progress of cell death, collectively gives insights into why cells can be susceptible to mechanical damage during cold transportation.

4. Conclusion

Findings from this initial study indicate that, for human mesenchymal stem cells, cell stiffness was altered with the progress of cell death after cold storage leading to susceptibility to mechanical cell damage. This is an important consideration for cell cold chain transportation. Additionally the range of stiffness measured within the sub-populations of dead cells may be the consequence of different modes of death, for example necrosis versus apoptosis. Further work with a larger number of cells will be required to confirm the phenomena observed with enhanced confidence.

Conflict of interest statement

All authors declare no conflict of interests.

Acknowledgements

Dr. N. Nikolaev was supported by the TSB, EPSRC and Loughborough University. Dr. Y. Liu was additionally supported by a UK Research Council Fellowship, Royal Society, FP7-PEOPLE-2012-IRSES (SkelGen) and EPSRC Centre for Innovative Manufacturing in Regenerative Medicine. We would also like to thank JPK for their support in providing access to their AFM facilities.

Appendix A. Supplementary material

Supplementary materials associated with this article can be found in the online version at http://dx.doi.org/10.1016/j.jbiomech.2013.12.004.

References

Abdelhady, S., Kitambi, S.S., Lundin, V., Aufschnaiter, R., Sekyrova, P., Sinha, I., Lundgren, K.T., Castelo-Branco, G., Linnarsson, S., Wedlich-Soldner, R., Teixeira, A., Andang, M., 2013. Erg channel is critical in controlling cell volume during cell cycle in embryonic stem cells. PloS One 8, e72409.

BILODEAU, G., 1992. Regular pyramid punch problem. J. Appl. Mech. Trans. ASME 59, 519–523.

Bortner, C., Cidlowski, J., 2002. Apoptotic volume decrease and the incredible shrinking cell. Cell Death Differ. 9, 1307–1310.

Chopinet, L., Roduit, C., Rols, M., Dague, E., 2013. Destabilization induced by electropermeabilization analyzed by atomic force microscopy. Biochim. Biophys. Acta-Biomembr. 1828, 2223–2229.

Darling, E.M., Topel, M., Zauscher, S., Vail, T.P., Guilak, F., 2008. Viscoelastic properties of human mesenchymally-derived stem cells and primary osteoblasts, chondrocytes, and adipocytes. J. Biomech. 41, 454–464.

Di Carlo, D., 2012. A mechanical biomarker of cell state in medicine. J. Lab. Autom. 17, 32–42.

Fuhrmann, A., Staunton, J.R., Nandakumar, V., Banyai, N., Davies, P.C.W., Ros, R., 2011. AFM stiffness nanotomography of normal, metaplastic and dysplastic human esophageal cells. Phys. Biol. 8, 015007.

Gonzalez-Cruz, R.D., Fonseca, V.C., Darling, E.M., 2012. Cellular mechanical properties reflect the differentiation potential of adipose-derived mesenchymal stem cells. Proc. Natl. Acad. Sci. USA 109, E1523–E1529.

Harris, A.R., Charras, G.T., 2011. Experimental validation of atomic force microscopy-based cell elasticity measurements. Nanotechnology 22, 345102.

Hemsley, A.L., Hernandez, D., Mason, C., 2011. Precisely delivered nanomechanical forces induce blebbing in undifferentiated mouse embryonic stem cells. J. Cell Health Cytoskelet. 3, 23–34.

Hessler, J.A., Budor, A., Putchakayala, K., Mecke, A., Rieger, D., Holl, M.M.B., Orr, B.G., Bielinska, A., Beals, J., Baker, J., 2005. Atomic force microscopy study of early morphological changes during apoptosis. Langmuir 21, 9280–9286.

Hu, M., Wang, J., Zhao, H., Dong, S., Cai, J., 2009. Nanostructure and nanomechanics analysis of lymphocyte using AFM: from resting, activated to apoptosis. J. Biomech. 42, 1513–1519.

Hur, S.C., Henderson-MacLennan, N.K., McCabe, E.R.B., Di Carlo, D., 2011. Deformability-based cell classification and enrichment using inertial microfluidics. Lab Chip 11, 912–920.

Jacobs, C.R., Huang, H., Kwon, R.R., 2013. Cell mechanics in the laboratory, Garland Science. Taylor & Francis, New York p. 185.

Johnson, K.L., 1985. Normal Contact of Elastic Solids – Hertz Theory. Cambridge University Press, Cambridge, pp. 91–99.

JPK Instrument AG, 2012. DP Data Processing Software Manual. 4.2, 85.

Kasas, S., Longo, G., Dietler, G., 2013. Mechanical properties of biological specimens explored by atomic force microscopy. J. Phys. D Appl. Phys. 46, 133001.

Kiessling, T.R., Stange, R., Kaes, J.A., Fritsch, A.W., 2013. Thermorheology of living cells-impact of temperature variations on cell mechanics. N. J. Phys. 15, 045026.

Lam, W.A., Rosenbluth, M.J., Fletcher, D.A., 2007. Chemotherapy exposure increases leukaemia cell stiffness. Blood 109, 3505–3508.

Lee, G.Y.H., Lim, C.T., 2007. Biomechanics approaches to studying human diseases. Trends Biotechnol. 25, 111–118.

Li, Q.S., Lee, G.Y.H., Ong, C.N., Lim, C.T., 2008. AFM indentation study of breast cancer cells. Biochem. Biophys. Res. Commun. 374, 609–613.

Lieber, S.C., Aubry, N., Pain, J., Diaz, G., Kim, S.J., Vatner, S.F., 2004. Aging increases stiffness of cardiac myocytes measured by atomic force microscopy nanoindentation. Am. J. Physiol. Heart Circ. Physiol. 287, H645–H651.

Lulevich, V., Shih, Y., Lo, S.H., Liu, G., 2009. Cell tracing dyes significantly change single cell mechanics. J. Phys. Chem. B 113, 6511–6519.

Lulevich, V., Yang, H., Isseroff, R.R., Liu, G., 2010. Single cell mechanics of keratinocyte cells. Ultramicroscopy 110, 1435–1442.

MacQueen, L.A., Thibault, M., Buschmann, M.D., Wertheimer, M.R., 2012. Electromechanical deformation of mammalian cells in suspension depends on their cortical actin thicknesses. J. Biomech. 45, 2797–2803.

Maloney, J.M., Nikova, D., Lautenschlaeger, F., Clarke, E., Langer, R., Guck, J., Van Vliet, K.J., 2010. Mesenchymal stem cell mechanics from the attached to the suspended state. Biophys. J. 99, 2479–2487.

Nawaz, S., Sanchez, P., Bodensiek, K., Li, S., Simons, M., Schaap, I.A.T., 2012. Cell visco-elasticity measured with AFM and optical trapping at sub-micrometre deformations. Plos One 7, e45297.

Nikolaev, N.I., Liu, Y., Hussein, H., Williams, D.J., 2012. The sensitivity of human mesenchymal stem cells to vibration and cold storage conditions representative of cold transportation. J. R. Soc. Interface 9, 2503–2515.

Ofek, G., Natoli, R.M., Athanasiou, K.A., 2009. In situ mechanical properties of the chondrocyte cytoplasm and nucleus. J. Biomech. 42, 873–877.

Rico, F., Roca-Cusachs, P., Gavara, N., Farre, R., Rotger, M., Navajas, D., 2005. Probing mechanical properties of living cells by atomic force microscopy with blunted pyramidal cantilever tips. Phys. Rev. E 72, 021914.

Rosenbluth, M.J., Lam, W.A., Fletcher, D.A., 2006. Force microscopy of nonadherent cells: a comparison of leukaemia cell deformability. Biophys. J. 90, 2994–3003.

Shimizu, Y., Haghparast, S.M.A., Kihara, T., Miyake, J., 2012. Cortical rigidity of round cells in mitotic phase and suspended state. Micron 43, 1246–1251.

Starodubtseva, M.N., 2011. Mechanical properties of cells and ageing. Ageing Res. Rev. 10, 16–25.

Tan, Y., Kong, C., Chen, S., Cheng, S.H., Li, R.A., Sun, D., 2012. Probing the mechanobiological properties of human embryonic stem cells in cardiac differentiation by optical tweezers. J. Biomech. 45, 123–128.

Targosz-Korecka, M., Biedron, R., Szczygiel, A.M., Brzezinka, G., Szczerbinski, J., Zuk, A., 2012. Stiffness changes of tumor HEp2 cells correlates with the inhibition and release of TRAIL-induced apoptosis pathways. J. Mol. Recognit. 25, 299–308.

Titushkin, I., Cho, M., 2007. Modulation of cellular mechanics during osteogenic differentiation of human mesenchymal stem cells. Biophys. J. 93, 3693–3702.

Wang, D., Chen, K., Tsai, C., Chen, G., Chen, C., 2011. AFM membrane roughness as a probe to identify oxidative stress-induced cellular apoptosis. J. Biomech. 44, 2790–2794.

Wang, J., Wan, Z., Liu, W., Li, L., Ren, L., Wang, X., Sun, P., Ren, L., Zhao, H., Tu, Q., Zhang, Z., Song, N., Zhang, L., 2009. Atomic force microscope study of tumor cell membranes following treatment with anti-cancer drugs. Biosens. Bioelectron. 25, 721–727.

Zahn, J.T., Louban, I., Jungbauer, S., Bissinger, M., Kaufmann, D., Kemkemer, R., Spatz, J.P., 2011. Age-dependent changes in microscale stiffness and mechanoresponses of cells. Small 7, 1480–1487.